Post-Miocene landscape rejuvenation at the eastern end of the Alps

Nicolas Legrain[1], Jean Dixon[2,†], Kurt Stüwe[1,*], Friedhelm von Blanckenburg[2,3], and Peter Kubik[4]
[1]INSTITUTE OF EARTH SCIENCES, UNIVERSITY OF GRAZ, UNIVERSITÄTSPLATZ 2, 8010, GRAZ, AUSTRIA
[2]HELMHOLTZ CENTRE POTSDAM, GERMAN RESEARCH CENTRE FOR GEOSCIENCES (GFZ), TELEGRAFENBERG, 14473 POTSDAM, GERMANY
[3]DEPARTMENT OF GEOSCIENCES, FREIE UNIVERSITÄT, BERLIN 12249, GERMANY
[4]LABORATORY FOR ION BEAM PHYSICS, ETH ZÜRICH, ZÜRICH CH-8093, SWITZERLAND

ABSTRACT

In the debate on the causes of uplift and landscape evolution of the Alps, most studies focus on regions that were glaciated at some stage during the last 2 m.y. In these areas, it is difficult to separate glacial-driven versus tectonically driven rates of erosion. Here, we present ^{10}Be-derived erosion rates from unglaciated catchments in the Koralpe range at the eastern end of the Alps. This region features strong geomorphologic evidence for landscape transience with young valleys incised into a smooth relict landscape. Erosion rates average 49 ± 8 mm/k.y. for catchments located on the relict landscape and 137 ± 15 mm/k.y. for catchments in the incised landscape. From these data, we estimate the onset of incision at 4 ± 1 Ma, the surface uplift at 350 ± 90 m, and a total relative base-level fall of 540 ± 140 m. Our results are in close agreement with both the magnitude and the age of onset of uplift of the Styrian Basin and the northern Molasse Basin, as well as the incision rate of the Mur River into the Styrian karst. The inferred timing of the onset of uplift around 4 Ma relates to interpreted basin inversion in the Pannonian Basin. Since this uplift event appears to have involved both the Pannonian Basin and the entire eastern end of the Alpine mountain range, we suggest that it may have occurred in response to a deep-seated process in the lithosphere. As such, we argue for tectonic drivers for the post-Miocene uplift in the eastern Alps.

LITHOSPHERE; v. 7; no. 1; p. 3–13 | Published online 17 October 2014 doi:10.1130/L391.1

INTRODUCTION

The recent topographic evolution of the European Alps and its relationship to climate and tectonics remain strongly debated (e.g., Cederbom et al., 2004, 2011; Herman et al., 2013; Baran et al., 2014). In this debate, no consensus has emerged about the relative tectonic versus climatic significance of the driving forces responsible for the last stages of uplift, in particular those in post-Miocene times (Dunkl et al., 2005; Wagner et al., 2010; Hergarten et al., 2010; Willett, 2010; Delunel et al., 2010; Wittmann et al., 2007; Kuhlemann et al., 2002; Champagnac et al., 2007; Legrain et al., 2014).

Some studies have argued that a significant part of the post-Miocene rock uplift in the Swiss Alps can be attributed to climatic drivers: For example, Wittmann et al. (2007), Champagnac et al. (2007), Sternai et al. (2012), and Norton et al. (2010a) suggested that Pliocene–Pleistocene glacial carving resulted in erosion-driven uplift, and that this uplift is an effect of long-term landscape transience due to the repeated glacial-interglacial cycles. At the eastern end of the Alps, glacial carving was minimal, but a Pliocene–Pleistocene uplift event is recognized nevertheless (e.g., Wagner et al., 2010). This finding suggests that for the eastern Alps, a tectonic cause for the recent uplift pattern should not be excluded. This argument is consistent with most recent suggestions by Baran et al. (2014) or Cederbom et al. (2011) and a series of other recent studies (e.g., Cloetingh et al., 2006).

In order to place better constraints on this debate, the magnitude and the regional distribution of recent uplift and erosion in the Alps need to be documented in regions where glacial erosion can largely be excluded. The Koralpe range at the eastern end of the Alps is such a region, because it remained unglaciated except for isolated small cirque glaciers around the highest peaks (Fig. 1). More than 90% of the Koralpe range, including summits above 2000 m elevation, features a fluvial landscape that has been interpreted as an incised relict landscape of Miocene age (Robl et al., 2008; Legrain et al., 2014). The region therefore represents a unique opportunity to investigate young uplift processes and place them into the framework of the post-Miocene erosion and rock uplift increase in the Alps.

Here, we present ^{10}Be-derived denudation rates (in this paper, these are also referred to as "erosion rates") from different parts of the Koralpe landscape in order quantify landscape-forming processes in a range that features transient incision into a relict landscape. In particular, we determined erosion rates from "old" and "young" parts of the landscape in order to test and quantify our earlier mapping results (Legrain et al., 2014). Then, we used the ^{10}Be-derived erosion rates for the two parts of the landscape and the known amount of incision into the relict landscape (Legrain et al., 2014) to calculate an estimate for the age of onset of incision and the amount of total relative base-level fall since onset of incision. We compared these results with different data sets from surrounding regions to explore if tectonic or climatic drivers may better explain the observed post-Miocene rock uplift increase in this part of the Alps. Finally, we inferred the topographic evolution of the Koralpe range since the late Miocene and compared it with the recent topographic evolution of the rest of the Alps.

GEOLOGICAL SETTING

The Koralpe range is located at the eastern end of the Alps, at the transition to the Pannonian Basin (Fig. 1). It is bordered to the west by the

*Corresponding author: kurt.stuewe@uni-graz.at.
†Present address: Department of Earth Sciences, Montana State University, Bozeman, Montana 59717, USA.

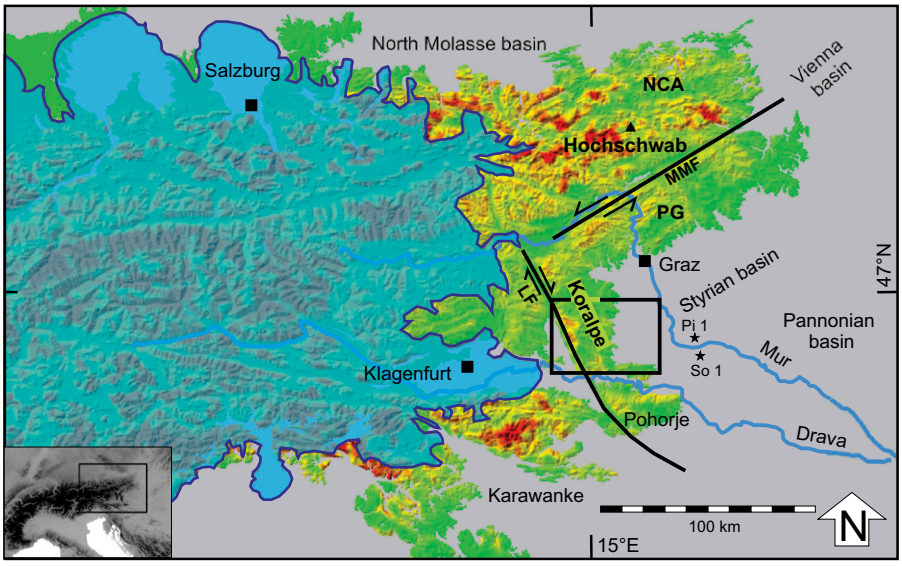

Figure 1. Map of the eastern end of the Alps (the region above 500 m elevation) showing the location of the Koralpe range. The black box delineates the region shown in detail in Figure 2. The blue semitransparent region reflects the extent of the Last Glacial Maximum (LGM) glaciation (van Husen, 1997). Color coding shows erosion rate (red—high ~0.5 mm/yr; green—low ~0.1 mm/yr) as predicted by the model of Hergarten et al. (2010) and calculated using the software from http://hergarten.at/geomorphology. This prediction is compared with the measured erosion rates presented in this paper. PG—Paleozoic of Graz; MMF—Mur-Mürz fault; LF—Lavanttal fault; NCA—Northern Calcareous Alps. Pi 1 and So 1 refer to wells "Pichla 1" and "Somat 1" used for subsidence analyses in the Styrian Basin (Ebner and Sachsenhofer, 1995), discussed in the text.

Lavanttal fault, one of the major strike-slip faults that had its peak of dextral strike-slip activity in the early Miocene, during the lateral extrusion of the eastern Alps (Ratschbacher et al., 1991; Frisch et al., 1998). The fault is a conjugate couple to the sinistral Mur-Mürz fault. Together, the two faults delineate the Styrian block to their east—a region inferred to have acted as a single coherent unit during the last few million years of tectonic evolution of the region (Wagner et al., 2011). The Styrian block includes both parts of the westernmost Pannonian Basin and its bordering ranges like the Koralpe. These bordering ranges also include the Styrian karst, which is part of the so-called "Paleozoic of Graz." In the Styrian karst, burial-age dating evidence from caves has been used to date some 600 m of uplift within the last 4 m.y. (Wagner et al., 2010), with the uplift rate being rapid at first and decreasing in the last 2 m.y. In the Pannonian Basin area of the Styrian block east of the Koralpe range (the Styrian Basin), a kilometer-thick sequence of Miocene sediments forms a hilly landscape around 300 m surface elevation. The Koralpe range itself consists of high-grade metamorphic rocks that experienced peak metamorphism at ~80 km depth around 90 Ma (Tenczer and Stüwe, 2003). Apatite fission-track ages document that the range was exhumed to near surface around 40–50 Ma (Hejl, 1997). (U-Th)/He thermochronology from the Koralpe range suggests a relatively steady exhumation from the Eocene to the Miocene of ~100 m/m.y. (Legrain et al., 2014; Hejl, 1997), but no more detailed resolution of the changes in uplift rate within the last few million years is known. During the early Miocene, the Koralpe range is interpreted to have been tilted eastward, with the tilting having occurred during the main activity of the Lavanttal fault—between 18 Ma and 16 Ma (Neubauer and Genser, 1990; Kurz et al., 2011; Legrain et al., 2014). The Lavanttal fault may have been active later (see Scharf et al., 2013), but the lack of tilting in geomorphological features indicates that this later activity involved no vertical motion (Legrain et al., 2014). Lithologically, the Koralpe range is composed of paragneisses and mylonitic gneiss, and it includes the type locality for the rock type eclogite (Fig. 2). There are also small marble lenses, but most rocks are very quartz rich and allow for ^{10}Be-derived erosion rates to be determined in all locations of the range.

Morphologically, the Koralpe region is characterized by two different areas: (1) a smooth, low-gradient relict landscape above roughly 1000 m elevation and reaching 2140 m on the highest point of the range (Speikkogel summit) and (2) a steeper, incised landscape below ~1000 m elevation, involving deeply incised valleys that successively dissect the range from the east and west sides (Legrain et al., 2014; Winkler-Hermaden, 1957; Frisch et al., 1998). Interpretation of channel profiles shows that the upland relict landscape is clearly separated from the incised landscape by knickpoints and can be mapped around the range (white line on Fig. 2; Legrain et al., 2014). However, note that the relict landscape itself contained substantial local relief even prior to the young uplift and incision event discussed here, so that local channels within the relict landscape may also contain steep sections. It was also shown that the incision into the relict landscape resulted from some 400 m of uplift and incision during the post-Miocene geological history of the region (Legrain et al., 2014). However, the timing of this uplift period remains unknown. During the glaciation periods of the last million years, and in particular during the Last Glacial Maximum (LGM), the Koralpe range was never pervasively glaciated (van Husen, 1997). Cirque glaciers around the highest peaks were small and isolated (Fig. 3B; van Husen, 1997), but they significantly disrupted the smooth surface of the relict landscape and created isolated glacial cirques with steep faces of up to 200 m height (Figs. 3C and 4). The local influence of these cirque glaciers on the Koralpe morphology is readily visible in terms of morphological features and moraine deposits. These areas were excluded from the interpretation presented here in order to avoid confusion with fluvially sculpted landscapes and the interpretation of their erosion rates. Today, the mean annual precipitation of Koralpe scales with elevation and ranges from 900 mm/yr at the lowest elevations to 1600 mm/yr in the summit area (http://www.zamg.ac.at).

METHODS

We determined catchment-wide erosion rates across the Koralpe range using the in situ–produced cosmogenic nuclide ^{10}Be. Nuclide concentrations in quartz integrate erosion rates over a 10^3 to 10^5 yr time scale (e.g., Granger et al., 1996). We sampled 21 rivers for cosmogenic ^{10}Be analysis, collecting sand from channel bottoms and active channel bars at several points along a 20 m reach at each stream location. Quartz was extracted from the 250–800 µm size fraction using magnetic separation and standard chemical leaching methods. We digested ~40 g of clean quartz in a 5:1 concentrated hydrofluoric acid:nitric acid mixture, along with 215 µg of a ^{9}Be carrier derived from a phenakite mineral. Beryllium was extracted from digested quartz using methods outlined in von Blanckenburg et al. (2004). We measured ^{10}Be/^{9}Be ratios on BeO targets with accelerator

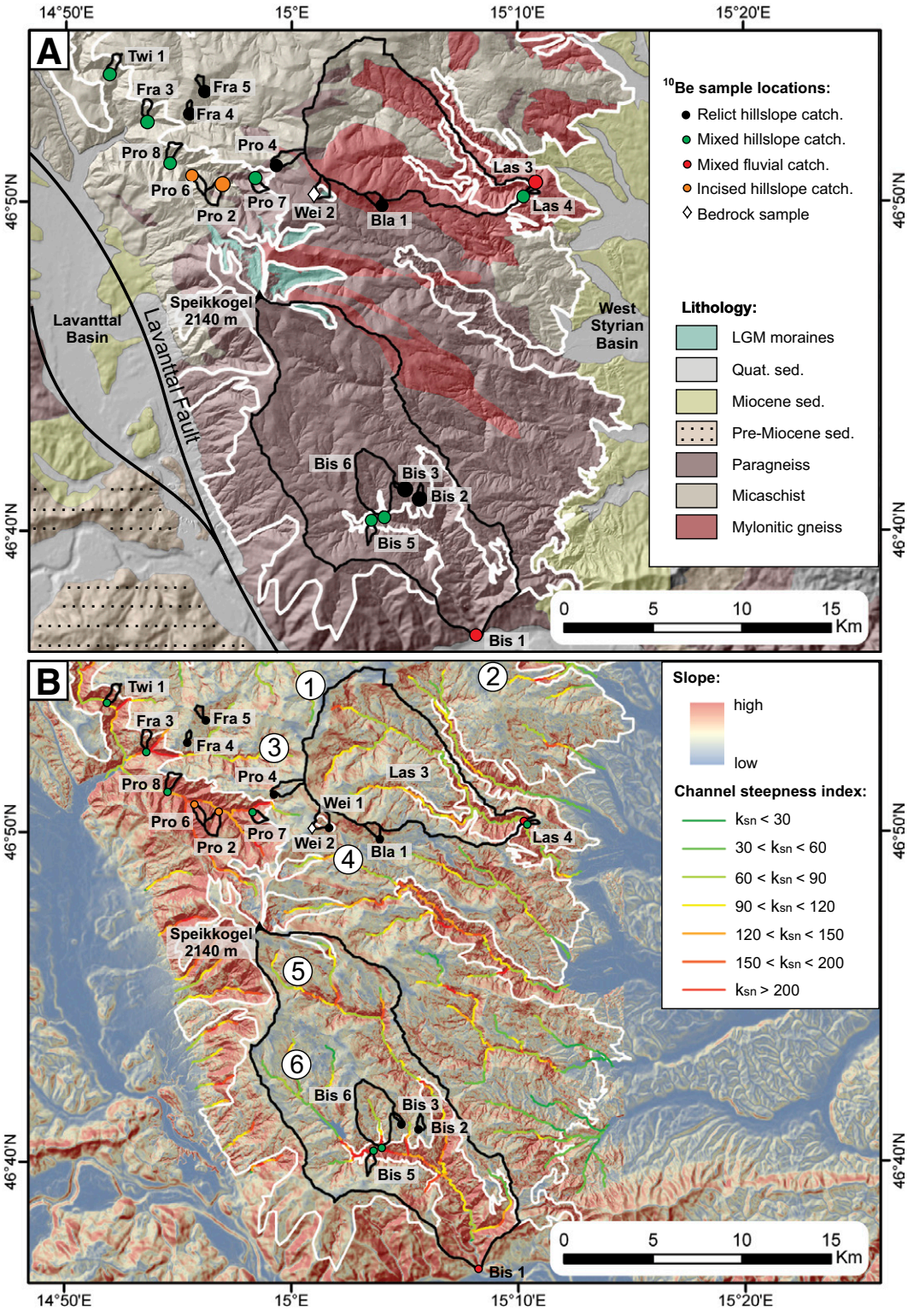

Figure 2. Map of the Koralpe range showing the location of river sediment samples. The thick white line represents the extent of the relict landscape as mapped by Legrain et al. (2014). (A) Location of the samples and simplified lithological map. Sampled catchments are shown as black lines. LGM—Last Glacial Maximum. (B) Spatial variation in slope and channel steepness index (color-coded river channels) calculated from a 10-m-resolution digital elevation model (DEM). Normalized channel steepness index (k_{sn}) was calculated with a reference concavity index of 0.45 and over 500 m segments. See Wobus et al. (2006) for definition of steepness and concavity index. Channels labeled with numbers are those discussed in connection with Table 2. They are: 1—Waldensteinerbach; 2—Fallegbach; 3—Frassbach; 4—Schwarze Sulm; 5—Krennbach; 6—Feistritz. Sampled catchments along the Prössingbach River are labeled "Pro."

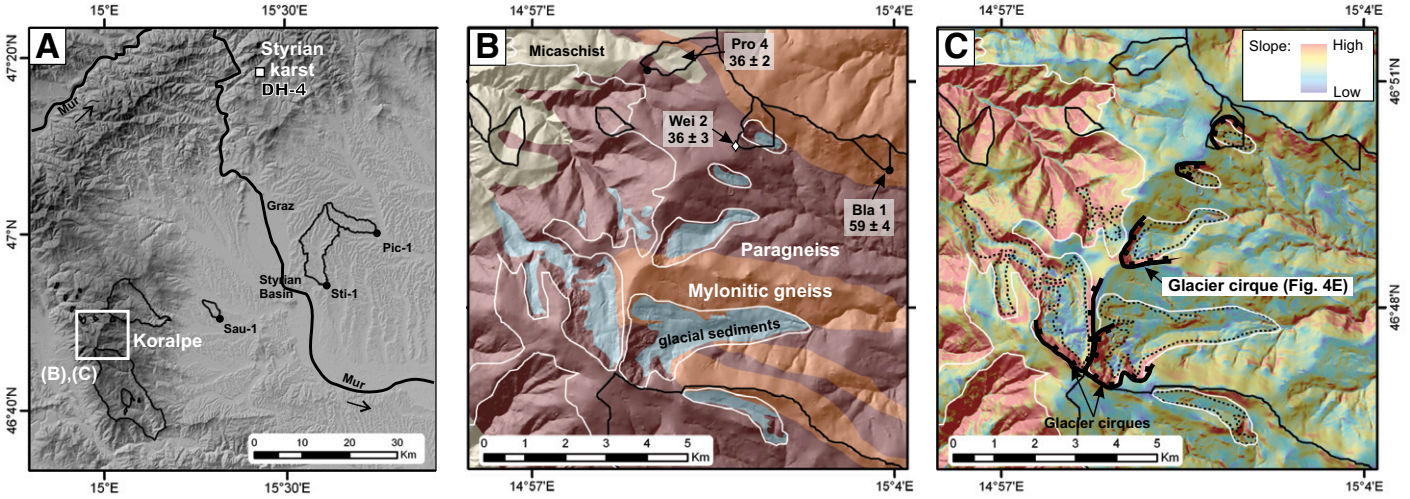

Figure 3. Location of samples in the Styrian Basin and evidence of glacial erosion on the upper part of the Koralpe relict landscape. (A) Location of catchments outside of Koralpe for which data are presented in this paper, and the location of sample DH4 from Wagner et al. (2010) in the Styrian karst. White box shows the area of B and C. (B) Lithology, extent of the Last Glacial Maximum (LGM) moraines, and measured erosion rates from the relict landscape in the upper part of the Koralpe range; white line shows the extent of the relict landscape. (C) Slope map and location of glacier cirques carved by LGM glaciers; dashed black lines show the extent of LGM moraines.

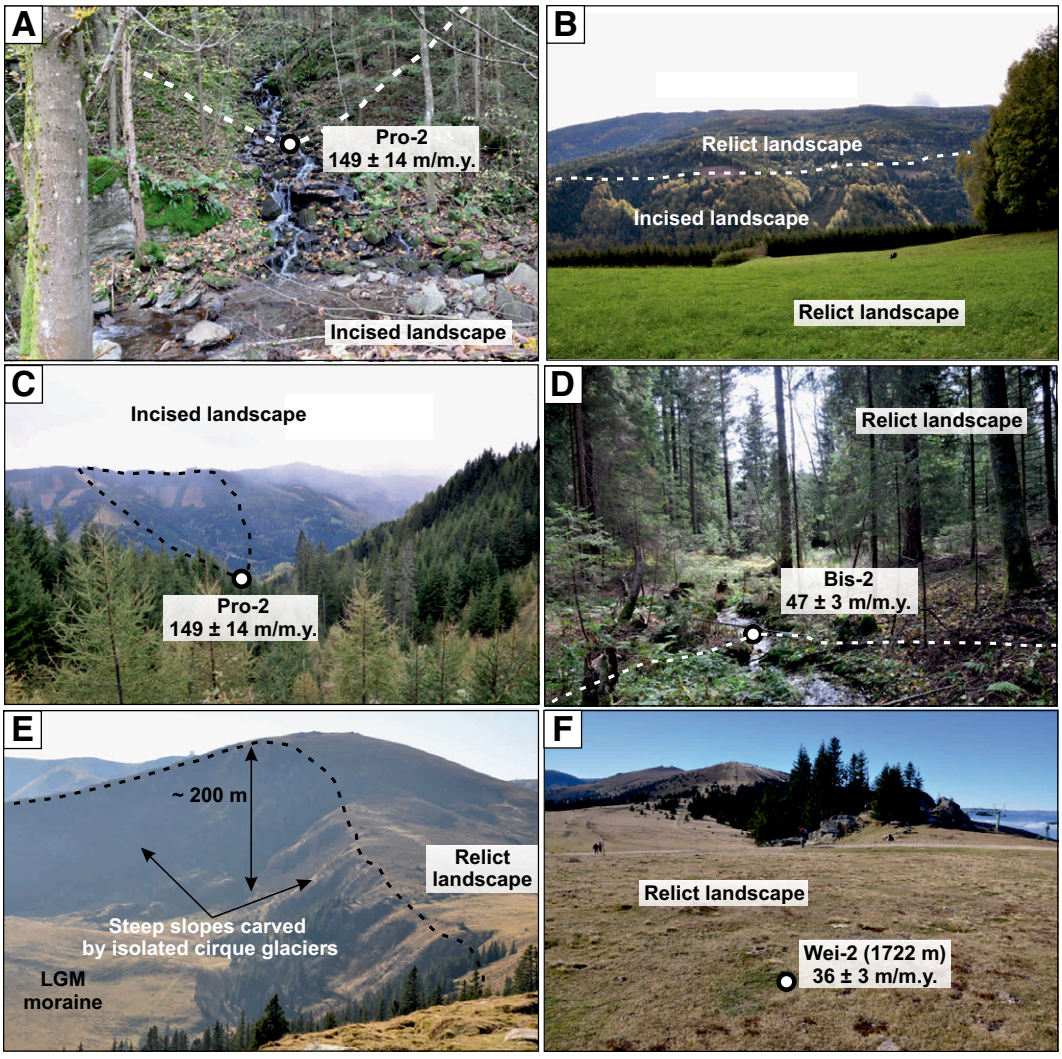

Figure 4. Photographs from the Koralpe range. (A) Sampling location of the highest erosion rate in the incised landscape of Koralpe; trunk stream in the foreground (Prössingbach river) flows from left to right. (B) View to the south in the Bistrica (Feistritz) catchment, approximately from the sampling location of Bis-3; break in slope separates the low-slope relict landscape from the steeper incised landscape below. (C) View of the entire catchment Pro-2 showing the steeper slope of the incised landscape (compare to photographs D and F). (D) View looking downstream of the sampling location of Bis-2 showing the gentle slopes of the Koralpe relict landscape hillslopes. (E) View looking south showing a glacier cirque carved by a 3-km-long Last Glacial Maximum (LGM) glacier into the relict landscape (see Fig. 3 for location of the cirque). (F) View to the south of the smooth crest of the Koralpe range forming part of the relict landscape.

mass spectrometry (AMS) at ETH Zürich in Switzerland in June 2010 and 2011. Initial AMS results were normalized to AMS standard S2007N, with an isotope ratio of 2.81×10^{-11}. All results were renormalized to the 07KNSTD standardization. The ^{10}Be concentrations were blank corrected (average ^{10}Be/^{9}Be ratio of five chemical processing blanks = $3.05 \pm 2.31 \times 10^{-15}$) by subtraction. Analytical results are presented in Table 1. The ^{10}Be concentrations were used to derive catchment-wide erosion rates following scaling factors from Dunai (2000) and absorption laws for nucleonic and muonic interactions from Schaller et al. (2002). Basin-averaged production rates were determined using 10 m gridded elevation data and using a sea-level, high-latitude production rate of 4.5 atoms/g quartz/yr. Corrections for skyline shielding were made following Norton and Vanacker (2009). In the absence of better information, snow shielding was calculated following Norton et al. (2011) using elevation–snow depth relationships determined in the Swiss Alps by Auer (2003). We set production rates equal to zero in parts of drainage basins where non-quartz-bearing lithologies were present (e.g., limestones). The ^{10}Be derived denudation rates and analytical data are presented in Table 1.

We divided sample locations into three categories based on the proportion of each catchment in the incised or relict portion of the Koralpe landscape, as described by Legrain et al. (2014) (white line on Fig. 2). Catchments were categorized as: "relict," "incised," and "mixed" (Table 1; Fig. 3). Relict and incised categories refer to catchments entirely located within these morphometric regions, and mixed landscape refers to catchments comprising both incised and relict parts of the landscape, as identified from mapping and quantitative geomorphic analysis by Legrain et al. (2014). For some of the sampled catchments, we also calculated erosion rates of nested catchments (Granger et al., 1996; Reinhardt et al., 2007):

TABLE 1. MORPHOMETRIC PARAMETERS AND CALCULATED ^{10}BE-DERIVED EROSION RATES OF SAMPLED CATCHMENTS

Sample	Long. (°E)	Lat. (°N)	Elevation (m)	Area (km²)	Slope† (°)	Fraction incised§	Sample weight (g)	^{10}Be concentration# (×10⁴ at/g quartz)	Topographic shielding factor	Snow shielding factor	Mean production rate††,§§ (at/g/yr)	Apparent age (ka)	Erosion rate (m/m.y.)	E^* ## (m/m.y.)
Relict landscape														
Wei-2§§§	15.015	46.836	1722	–	–	–	28.09	37.62 ± 2.31	1.00	0.89	19.05	16.67	36 ± 3	–
Fra-4	14.922	46.88	1084	0.11	12.7	0	26.89	20.00 ± 0.91	1.00	0.93	12.18	12.77	47 ± 3	–
Fra-5	14.934	46.89	1193	0.21	17.2	0	28.72	19.00 ± 0.87	0.99	0.92	13.88	10.91	55 ± 3	–
Pro-4	14.987	46.852	1476	0.91	12.9	0	32.58	34.46 ± 1.32	1.00	0.9	17.26	16.67	36 ± 2	–
Bla-1	15.063	46.831	1451	0.46	21	0	28.03	19.45 ± 0.93	0.98	0.91	15.49	10.17	59 ± 4	–
Bis-2	15.092	46.683	1047	0.24	10.3	0	28.73	19.00 ± 0.93	1.00	0.94	11.59	12.77	47 ± 3	–
Bis-3	15.081	46.686	1070	0.14	15.1	0	29.36	17.98 ± 0.80	1.00	0.93	11.85	11.77	51 ± 3	–
					14.9 ± 1.6†††								**49 ± 3†††**	
Mixed landscape														
Twi-1	14.862	46.899	556	0.45	23.3	0.74	27.77	8.72 ± 0.47	0.98	0.95	9.6	6.74	89 ± 6	109 ± 7
Fra-3	14.891	46.874	577	0.4	24.6	0.71	30.25	14.05 ± 0.66	0.97	0.95	9.91	10.71	56 ± 3	107 ± 7
Pro-7	14.971	46.844	1107	0.37	26.8	0.81	40.47	8.95 ± 0.54	0.97	0.91	14.49	4.88	123 ± 9	115 ± 8
Pro-8	14.908	46.854	623	0.48	27.6	0.86	40.48	12.75 ± 0.57	0.96	0.95	10.13	9.52	63 ± 4	118 ± 8
Las-4	15.173	46.838	701	0.1	28.3	0.66	29.84	9.78 ± 0.49	0.97	0.97	8.23	8.70	69 ± 4	102 ± 6
Bis-5	15.06	46.672	758	0.39	17.7	0.42	33.06	7.50 ± 0.45	0.99	0.94	11.06	5.13	117 ± 8	83 ± 6
Bis-6	15.066	46.673	734	5.84	16.9	0.05	40.24	11.70 ± 1.11	0.99	0.93	12.45	7.32	82 ± 9	53 ± 6
Bis-1	15.139	46.613	382	142	17.9	0.17	30.25	11.74 ± 0.87	0.99	0.92	11.7	8.70	69 ± 6	63 ± 5
Las-3	15.173	46.838	542	66	18.6	0.12	31.65	13.70 ± 0.60	0.99	0.92	12.08	9.84	61 ± 4	59 ± 3
					22.4 ± 2.2†††								**81 ± 9†††**	
Incised landscape														
Pro-2	14.945	46.844	866	0.81	27.8	1	30.31	6.72 ± 0.58	0.97	0.93	12.91	4.03	149 ± 14	–
Pro-6	14.927	46.848	737	0.45	29.4	1	40.78	8.24 ± 0.61	0.96	0.94	11.68	5.41	111 ± 9	–
Bis-1* ###	–	–	–	30	28	1	–	–	–	–	–	4.11	146 ± 7	–
Las-3* ###	–	–	–	8.19	27.7	1	–	–	–	–	–	4.20	143 ± 4	–
					28.2 ± 0.4†††								**137 ± 9†††**	
Styrian Basin														
Sti-1	15.591	49.905	304	68	9.3	–	31.23	4.35 ± 0.31	0.99	1.00	6.36	4.88	123 ± 9	–
Pic-1	15.75	47.003	326	28	10.4	–	30.70	4.91 ± 0.38	1.00	0.99	6.40	5.45	110 ± 9	–
Sau-1	15.311	46.842	317	6.6	5.9	–	40.14	15.47 ± 0.86	1.00	0.99	6.09	18.18	33 ± 2	–
					9.9 ± 0.6†††								**89 ± 28†††**	

†Catchment mean slope calculated from 10 m digital elevation model (DEM).
§Fraction of incised landscape within the catchment.
#^{10}Be concentrations measured at ETH-Zurich in June 2010 and 2011. Results are normalized to Nishiizumi et al. (2007) 2007KNSTD standard, corrected for average of five chemical processing blanks. Blank ^{10}Be/^{9}Be = $3.05 \pm 2.31 \times 10^{-15}$ (mean and standard deviation). Snow shielding was calculated from annual Swiss snow data (Auer, 2003). Topographic shielding was calculated on 10 m DEM.
††Based on compilation of high-latitude, sea-level production rates of 4.5, 0.097, and 0.085 atoms/g quartz/yr for high-energy neutrons, negative muons, and fast muons respectively.
§§Per-pixel production rates calculated for quartz-bearing lithologies following scaling laws of Dunai (2000) and Schaller et al. (2002) for nucleonic and muonic interactions. Catchment production rates include both topographic and snow-shielding correction factors.
##Modeled erosion rate (E^*) for mixed basins calculated based on end-member mixing model of incised and relict portions of the catchment (refer to text for more details).
†††Bold numbers reflect the mean and standard error of slope or erosion rate measurements for each landscape.
§§§Erosion rate of bedrock sample (Wei-2) not included in the mean erosion rate of the relict landscape.
###Incised portions of larger mixed catchments. See text for details.

$$\varepsilon_i = \frac{\varepsilon_e A_e - \varepsilon_r A_r}{A_i}, \quad (1)$$

where ε is erosion rate, A is the size of the catchment, and the subscripts e, i, and r refer to the entire catchment, the incised part of the catchment, and the relict part of the catchment, respectively. In addition to the erosion rates from the Koralpe range, we measured erosion rates from three catchments located in the Styrian Basin, east of the Koralpe range (Fig. 3A).

We also defined another classification of catchments based on the drainage area of the sampled catchments. Previous analysis of catchment morphology and log-slope, log-area relationships identified the critical drainage area for each catchment that separates portions of the landscape dominated by hillslope and fluvial processes (Legrain et al., 2014). We assumed a conservative critical area of 7 km^2 (in accordance with Legrain et al., 2014) for the Koralpe region. Based on these results from digital elevation model (DEM) analysis, we defined three categories based on drainage area of the catchments: bedrock sample ($A = 0$), small catchments ($A < 7$ km^2), and large catchments ($A > 7$ km^2). Combining both classifications, our ^{10}Be-derived erosion rate samples can be divided into five categories (Fig. 2; Tables 1 and 2): Samples from (1) relict small catchments (6 samples), (2) mixed small catchments (7 samples), (3) mixed large catchments (2 samples), (4) incised small catchments (2 samples), and (5) relict bedrock (1 sample) locations plus three samples from the Styrian Basin. There are no samples from incised large catchments ($A > 7$ km^2), as all larger catchments in the Koralpe contain at least some fraction from the relict landscape. However, we did calculate theoretical erosion rates for large incised catchments using the two largest samples from the "mixed" catchments and Equation 1.

RESULTS

The ^{10}Be-derived erosion rates from the Koralpe range from 36 mm/k.y. to 149 mm/k.y. (Fig. 5; Table 1). They are consistent with the long-term exhumation rate of ~100 m/m.y. since the Eocene as inferred from fission-track and (U-Th)/He ages (Hejl, 1997; Legrain et al., 2014) for the Koralpe range. Erosion rates show a clear difference between relict and incised landscape (Fig. 5B). The mean erosion rate of the incised catchments is more than 2.5 times higher than the mean erosion rate of the relict landscape (137 ± 15 mm/k.y. and 49 ± 8 mm/k.y., respectively; Table 1). Erosion rates from catchments within the Koralpe relict landscape range from 36 ± 3 mm/k.y. to 59 ± 4 mm/k.y. (Table 1). The erosion rates of the two entirely incised catchments are 111 ± 9 mm/k.y. (Pro 6) and 149 ± 14 mm/k.y. (Pro 2). Erosion rates of mixed catchments comprising both incised and relict landscape range from 56 ± 3 mm/k.y. to 123 ± 9 mm/k.y. and average 81 ± 24 mm/k.y.

Erosion rates from the Styrian Basin east of the Koralpe range are 33 ± 2 mm/k.y. to 123 ± 9 mm/k.y. (Fig. 6; Table 1). Two larger catchment (Sti-1 and Pic-1) exhibit similar erosion rates, while the small catchment sampled in the Styrian Basin (Sau-1) shows a low rate of 33 ± 2 mm/k.y. However, in general, the erosion rates from the Styrian Basin appear to be relatively high across our sample region and average 88 ± 40 mm/k.y (Table 1).

TABLE 2. CALCULATED TIME OF INCISION AND TOTAL BASE-LEVAL FALL

River name*	$\Delta z^{\dagger}$ (m)	$\Delta t_k^{\S}$ (m.y.)	$\Delta B_k^{\#}$ (m)
Waldensteinerbach	241 ± 22	2.7 ± 0.3	375 ± 23
Fallegbach	403 ± 67	4.6 ± 0.9	627 ± 69
Frassbach	216 ± 15	2.5 ± 0.3	336 ± 16
Schwarze Sulm	372 ± 76	4.2 ± 0.9	579 ± 79
Krennbach	480 ± 97	5.5 ± 1.2	747 ± 100
Feistritz	380 ± 56	4.3 ± 0.7	592 ± 58
μ ± s.d.	349 ± 92	4.0 ± 1.0	543 ± 143

*Selected channels are labeled in Figure 2 and correspond to those discussed by Legrain et al. (2014).
$^{\dagger}\Delta z$—amount of incision calculated from projection of six channels across Koralpe.
$^{\S}\Delta t_k$—time needed for the incision calculated as $\Delta t_k = \Delta z/(U_r - U_i)$ (Eq. 2). U_r and U_i are 137 ± 15 m/m.y. and 49 ± 8 m/m.y. respectively; see text for more details.
$^{\#}\Delta B_k$—amount of total relative base-level fall calculated with $U_i = 49 \pm 8$ m/m.y.

CORRELATION AND INTERPRETATION OF THE DATA

Erosion rate data exhibit poor correlation with mean catchment slope (Fig. 5A), and plotted together, they do not support correlation models previously shown in other mountainous landscapes (e.g., Montgomery and Brandon, 2002; DiBiase et al., 2010; Carretier et al., 2013; Abbühl et al., 2011). However, these relationships become more clear when we divide our sampled catchments into the previously identified classifications based on size and degree of incision. For example, the correlation of erosion rate with mean catchment slope is notably more scattered for data from mixed small catchments than for incised small or relict small catchments (Fig. 5A). Overall, there is a positive linear correlation of erosion rate with the fraction of incised landscape within the catchment ($r^2 = 0.49$; Fig. 5B). The correlation coefficient omitting the mixed small catchments is significantly better ($r^2 = 0.90$; $n = 10$) than the correlation coefficient for all the data ($r^2 = 0.49$; $n = 17$).

The erosion rate data suggest that the relationships between landscape morphology and erosion rates are modulated by catchment size. Incised and relict portions of catchments each reflect distinct geomorphic processes. In large mixed catchments, the erosional expression of these processes is averaged out across the basin. However, we suggest that the heterogeneity of processes eroding small mixed catchments is not similarly averaged out due to the catchment size. Instead, erosion rates within these

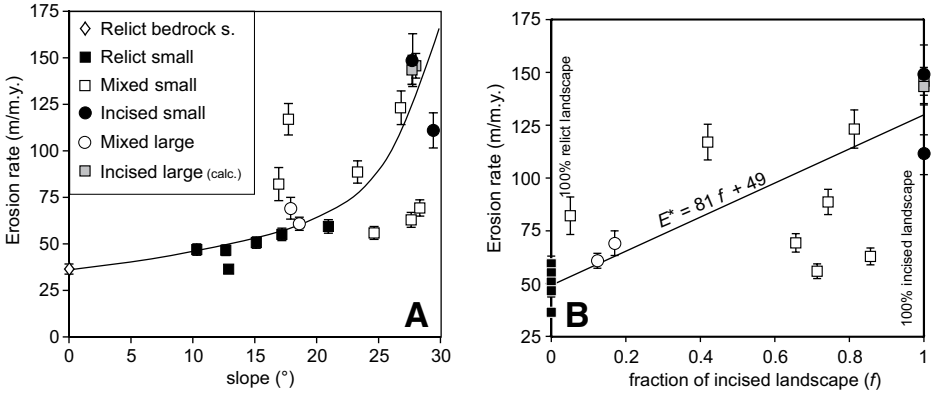

Figure 5. Plots of erosion rate vs. different geomorphic parameters. (A) Erosion rate vs. mean slope of the catchments; black line is a fit of the data with a nonlinear model of Montgomery and Brandon (2002). While we acknowledge that this model was derived from a much coarser-resolution data set, and other models exist, we emphasize that the model is for reference only, and the density of our data set does not justify more elaboration on the fit. (B) Erosion rate vs. fraction of incised landscape within the catchments. The equation and line represent the best linear fit to the end-member incised and relict catchment samples.

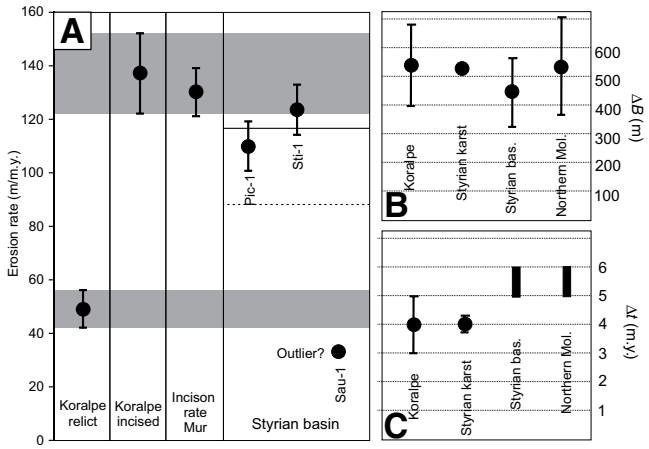

Figure 6. Comparison between millennial-scale ^{10}Be-derived erosion rates from the Koralpe range and Styrian Basin and the inferred long-term incision rate of the Mur River in the Styrian karst (Wagner et al., 2010), calculated as the average incision rate across the last 4 m.y. (A) Lower and upper gray areas represent the average erosion rate of the Koralpe relict and incised landscapes, respectively, with standard deviation around the mean. (B–C) Comparison between total relative base-level fall (ΔB) and duration for the incision (Δt) from Koralpe, the Styrian karst, and the Styrian Basin. Data point for the Styrian karst (incision rate of Mur) is derived from sample DH4 of Wagner et al. (2010); data points for the Styrian Basin are calculated from wells (Ubersbach 1, Radkersburg 2, Pichla 1, Somat 1—Ebner and Sachsenhofer, 1995; Sachsenhofer et al., 1998). Data points for the northern Molasse Basin are also calculated from wells (Strh 1, Stkr 1, Fü 3, Mlbg 1, Stbg 1, Li 1, Di 1, St 1, He 3—Genser et al., 2007).

catchments capture the true spatial and temporal variability of erosion, as caused, for example, by rock type, jointing, local discharge, weathering, or the local degree of transient incision and hillslope response. A similar dependence of catchment size on erosion rate variability was previously demonstrated for the central Alpine Maggia Valley (Wittmann et al., 2007; Figs. 5 and 6).

In order to improve on the understanding of the correlation between erosion rate and proportion of the incised landscape in a catchment, we calculated theoretical erosion rates (E^*) for mixed catchments based on a linear fit between the two end-member erosion settings (Fig. 5B). We defined these two end-member settings by the mean erosion rate of all measured catchments that are located either in 100% incised or 100% relict landscapes, respectively (incised catchments; $n = 2$; $E^* = 130$ mm/k.y.; relict catchments: $n = 6$; $E^* = 49$ mm/k.y.). The erosion rate E^* is given by: $E^* = 81f + 49$, where f is the fraction of incised landscape within the catchment (Fig. 5B; Table 1). We see that all mixed catchments feature erosion rates between these two end members, a finding similar to that of Van den Berg et al.,(2012) in the central Alps. The fact that mixed small catchments scatter significantly around the predicted value is consistent with the idea of small catchments expressing their local conditions and local erosion response. Interestingly, end-member catchments (100% relict small or 100% incised small catchments) that are smaller than this critical catchment size do not feature this variability—possibly because these portions of the landscape have attained a geomorphic equilibrium, such that catchments within each setting erode at the same rate.

Using Equation 1 to calculate erosion rates for the incised parts of large mixed catchments (Bis-1* = 146 ± 7 mm/k.y. and Las-3* = 143 ± 8 mm/k.y.), we find that the modeled erosion rates are consistent with measured rates for the small catchments entirely located in the incised landscape (Table 1; Pro-6 = 111 ± 9 mm/k.y. and Pro-2 = 149 ± 14 mm/k.y.). It is important to note that these two types of erosion rates are measured independently from each other. Therefore, the average of these four erosion rates (137 ± 15 mm/k.y.) should represent the erosion rate of the incised landscape of Koralpe (Fig. 6).

Erosion rates of two large catchments (Pic-1 and Sti-1) in the Styrian Basin average 117 mm/k.y. This value is comparable to the mean erosion rate of the Koralpe incised landscape (137 ± 15 mm/k.y; Fig. 6) and also to the long-term incision rate determined for this region from cosmogenic dating of cave sediments in Styrian karst (Wagner et al., 2010). This agreement suggests that the Styrian Basin is currently responding to a relative base-level fall that is transmitted to the Koralpe range but has not yet reached the relict landscape. This is logical if the Styrian Basin and the Koralpe range respond to a common rock uplift process as parts of the Styrian block.

Channel and Hillslope Adjustment to a Sudden Base-Level Drop

The processes of successive adjustment of a catchment to a new base level can be explored in more detail by investigating a large mixed catchment that crosses both the relict and the incised landscape. The Prössingbach catchment northwest of the Koralpe summit is the most incised of the large Koralpe catchments (Fig. 2). It is therefore a good area to investigate how channel, hillslopes, and erosion rates adjust to increased uplift rates and associated base-level drop (Fig. 7).

Hillslope and channel morphology of the Prössingbach River show a clear separation between the upper relict landscape and the lower incised landscape. The river network in the channel shows a prominent knickpoint at this transition (Fig. 7). Interestingly, the mean slope of small tributary catchments connected to the Prössingbach River increase sharply 1.5 km downstream of the knickpoint (Figs. 7A and 7D). The spatial lag between the knickpoint and the increase in slope of adjacent hillslopes is inferred to reflect a temporal lag by the time needed for the hillslopes to propagate the incision signal upstream and increase the mean slope of the catchment.

The erosion rates of tributary catchments correlate well with the mean slope of the catchments, and the transition from incised to relict portions of the landscape. Erosion rates in the two relict catchments (36 mm/k.y.) are several factors lower than those of two incised catchments (average of 130 mm/k.y.; Fig. 7E). As above, the mixed hillslope catchments Pro-8 and Pro-7 are interpreted as scattering values between the two erosion rate signals.

The time response of hillslopes can be estimated by the distance between the knickpoint and the downstream location where the hillslopes within a tributary catchment are entirely within the incised portion of the landscape. These hillslopes have propagated the entire erosion signal up to the crest. The assumption is that the shorter is the distance, the faster is the time response (Hurst et al., 2012). For the Prössingbach catchment, one would therefore infer that the hillslope response time is different between the north- and south-facing hillslopes. Indeed, in downstream tributaries such as Pro-8, which is located 9 km downstream of the knickpoint, the incision wave has not yet propagated up to the crest, while hillslopes located south of the Prössingbach River are entirely incised only ~3 km downstream of the knickpoint (Fig. 7A). However, these differences between north-facing and south-facing catchments might also be explained by the geometry of the fluvial network of this catchment, since southern tributaries joining the Prössingbach River are larger than those on the north side (Figs. 2 and 7A).

DISCUSSION

The data presented here provide several important constraints on the uplift of the Koralpe region. In particular, the difference in erosion rates

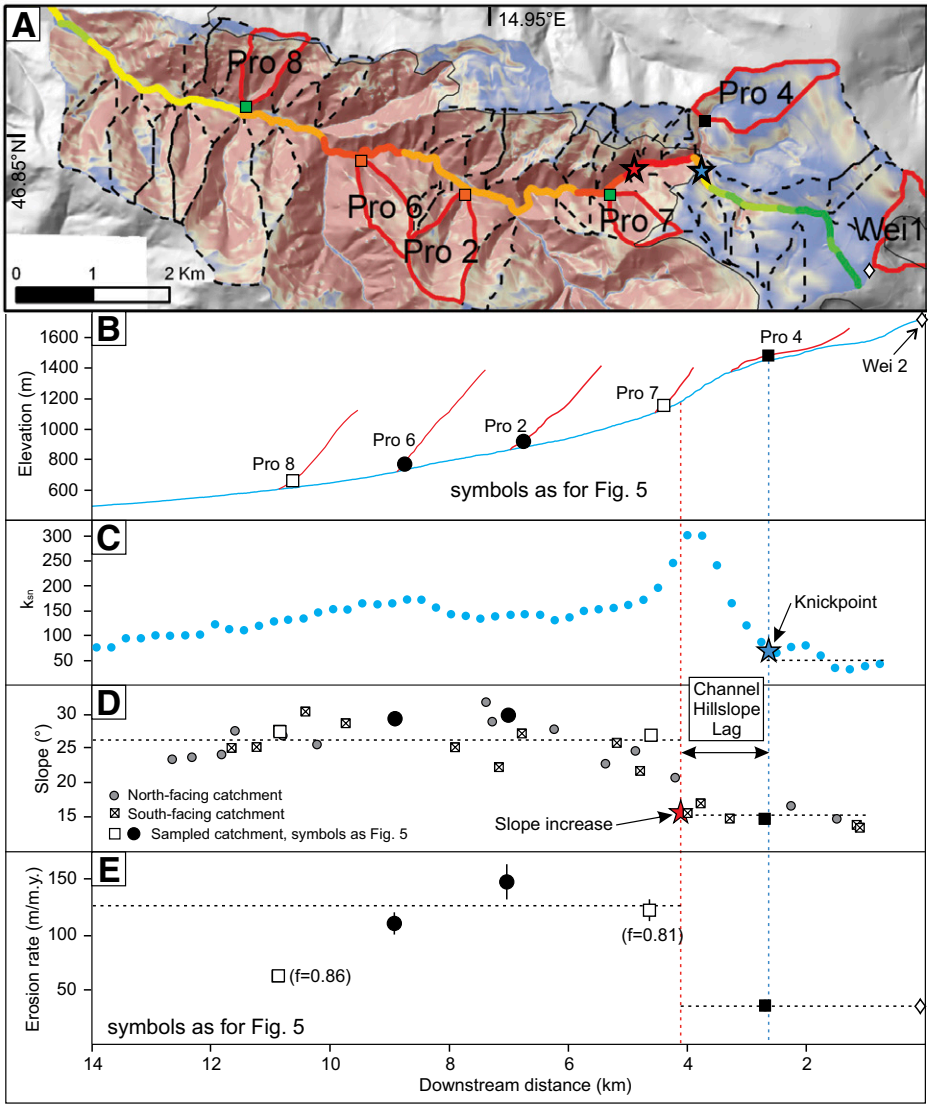

Figure 7. Morphology and erosion rates of the Prössingbach River. (A) Map of the catchment (dashed black lines) with the sampled basins (red lines). Color coding for the slope base map increases from blue to red, while color coding of the channel reflects increasing k_{sn} from green to red (for definitions, see Wobus et al., 2006). (B) Channel profile of the Prössingbach River and sampled tributaries. (C) Along-stream variation of k_{sn} for the Prössingbach River calculated with a reference concavity of 0.45 and along 500 m segments. (D) Along-stream variation of mean slope of tributary catchments. Horizontal dashed line is the mean slope of tributary catchments, marked by dashed with black line on A. (E) Along-stream variation of erosion rate of the sampled tributaries catchments, where *f* is fraction of incised landscape for the mixed samples, and dashed black lines are average erosion rate of incised (Pro-2, Pro-6) and relict (Pro-4, Wei-2) samples for the two parts of the landscape.

between the two parts of the Koralpe landscape clearly shows that the landscape is currently adjusting to a wave of incision. We infer that rock uplift is largely equal to erosion for the Styrian Basin (assuming almost no surface uplift), so that the basin's elevation remains approximately constant at the level of the regional base level, while the Koralpe is a transient landscape currently responding to recent uplift. The causes of the uplift and incision of the entire region and timing are discussed next.

Timing of Incision for the Koralpe

When a sudden increase in rock uplift occurs in a previously equilibrated landscape (where rock uplift and erosion rate are in balance), then the initial and final rock uplift rates U_i and U_f are connected to the initial (R_i) and final relief (R_f), respectively. Channels in the incised part of the landscape will adjust their erosion rate to U_f, whereas channels in the relict landscape will still erode at rates comparable to U_i (Kirby and Whipple, 2012). When U_i, U_f, and the amount of incision (Δz) are known (and horizontal erosion and advection processes are neglected), it is possible to calculate the time (Δt_k) needed for the incision (Whipple and Tucker, 1999; Kirby and Whipple, 2012; Miller et al., 2013):

$$\Delta t_k = \Delta z / \left(U_f - U_i\right). \quad (2)$$

Correspondingly, the total relative base-level fall (ΔB_k) can be calculated by adding the amount of erosion of the relict landscape since the beginning of uplift to the measured amount of incision from channel projection:

$$\Delta B_k = \Delta z + \left(U_i \times \Delta t_k\right). \quad (3)$$

Based on these relationships and the known amount of incision (Δz = 350 ± 90 m; from Legrain et al., 2014), we used a simple two-stage uplift model for the Koralpe region to define the different vertical motions (rock uplift, surface uplift, erosion) across the study area (Fig. 8). We also compared the incision of the Koralpe relict landscape with three other data sets: (1) the incision record of the Mur River in the Styrian karst as measured from burial age dating of cave sediments by Wagner et al. (2010), (2) subsidence analysis of the Styrian Basin (Ebner and Sachsenhofer, 1995; Sachsenhofer et al., 1998), and (3) subsidence analysis of the northern Molasse Basin (Genser et al., 2007). For the Koralpe, Δz represents the amount of incision since the rock uplift increase and ΔB_k is the total amount of base-level fall since the onset of rock uplift, also equivalent to

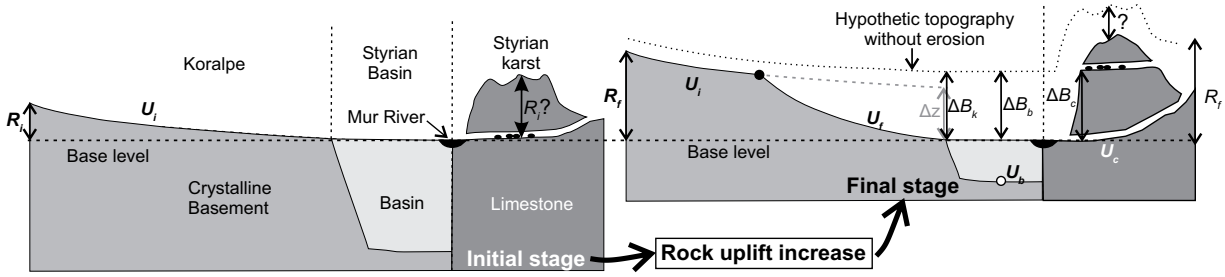

Figure 8. Schematic cross section through the Koralpe, Styrian Basin, and Styrian karst regions showing a simplified model of uplift for the studied region with definition of variables. Note that the scale is exaggerated for illustration, especially R_f and R_i for Koralpe. U_f—rock uplift rate final; U_i—rock uplift rate initial; U_b—uplift rate Styrian basin; U_c—Uplift rate Styrian karst; ΔB_k—total relative base level fall; ΔB_b—relative base level fall Styrian basin; ΔB_c—relative base level fall Styrian karst; R_f—relief final; R_i—relief initial.

the total amount of rock uplift since the uplift increase (Fig. 8). Subsidence analyses in the Styrian Basin by Ebner and Sachsenhofer (1995) have constrained some of these vertical motions in the Styrian block, and we use their results as a proxy for uplift.

Using these model and variables, we calculated the base-level fall and its timing for the Koralpe range using Equations 2 and 3. For the values of U_i and U_f, we used the average erosion rate of the catchment from the relict landscape (49 ± 8 mm/k.y.) and the average erosion rate from the incised landscape catchments (137 ± 15 mm/k.y.), respectively (Tables 1 and 2). Calculations yield an incision time $\Delta t_k = 4.0 \pm 1.0$ Ma and a total relative base-level fall $\Delta B_k = 540 \pm 140$ m since the beginning of incision (Table 2). This timing of incision can be interpreted as the minimum age for the onset of incision because only the vertical incision is taken into account with Equation 3. Lateral knickpoint migration is neglected, and the calculated time of incision could be shorter than the real onset of incision.

Our estimates of $\Delta t_k = 4.0 \pm 1.0$ Ma and $\Delta B_k = 540 \pm 140$ m are based on the assumption that erosion rates have been constant across the averaging time scale of ^{10}Be-derived erosion rates (4–18 ka for our catchments). This assumption appears problematic because climate has changed repeatedly in the last million years, so that changes within the time-averaging of the method are expected. However, support for this assumption is provided by a comparison between short-term erosion from the Koralpe incised landscape and the long-term incision rate of the Mur River in the Styrian karst averaged over the last 4 m.y. (Wagner et al., 2010). Wagner et al. (2010) interpreted a detailed incision history of the Mur River for the last 4 m.y. and derived a mean incision rate of 130 ± 9 m/m.y. based on the oldest cave sediments (Fig. 3A; e.g., sample DH4: 4.05 ± 0.28 Ma). The close match between the ^{10}Be-derived erosion rate of the Koralpe incised landscape (137 ± 15 mm/k.y.) and the long-term incision rate of the Mur River (130 ± 9 m/m.y. of Wagner et al., 2010) strongly supports the assumption that the ^{10}Be derived-erosion rates of Koralpe are representative of the long-term erosion rates.

Our results and interpretation regarding the magnitude and timing of uplift can also be compared to the subsidence record of wells from both the Styrian Basin (Ebner and Sachsenhofer, 1995; Sachsenhofer et al., 1998) and the northern Molasse Basin (Genser et al., 2007). For the Koralpe region, we calculated a total relative base-level fall of ~540 ± 140 m. This change is similar to the calculated base-level fall in the Styrian karst ($\Delta B_c = 543$ m). Additionally, the base-level fall in the Styrian Basin ($\Delta B_b = 440 \pm 100$) is comparable within error to that in the northern Molasse Basin north of the region investigated here ($\Delta B_k = 540 \pm 170$ m; Fig. 8; see Genser et al., 2007). The similarity between these four independent data sets suggests that the entire region may have responded at approximately the same time (between 6 Ma and 4 Ma) to an increase in rock uplift rate, with a relative base-level fall of ~500 m following uplift (Fig. 8). Figure 9 shows the spatial distribution of the amount of rock uplift for the different wells as derived from subsidence analyses of Ebner and Sachsenhofer (1995), Sachsenhofer et al. (1998), and Genser et al. (2007) near the eastern end of the Alps.

Post-Miocene Rock Uplift Increase in the Eastern Alps

While climate has been invoked as a driver of uplift in other portions of the Alps (e.g., Wittmann et al., 2007), a climate-related post-Miocene uplift

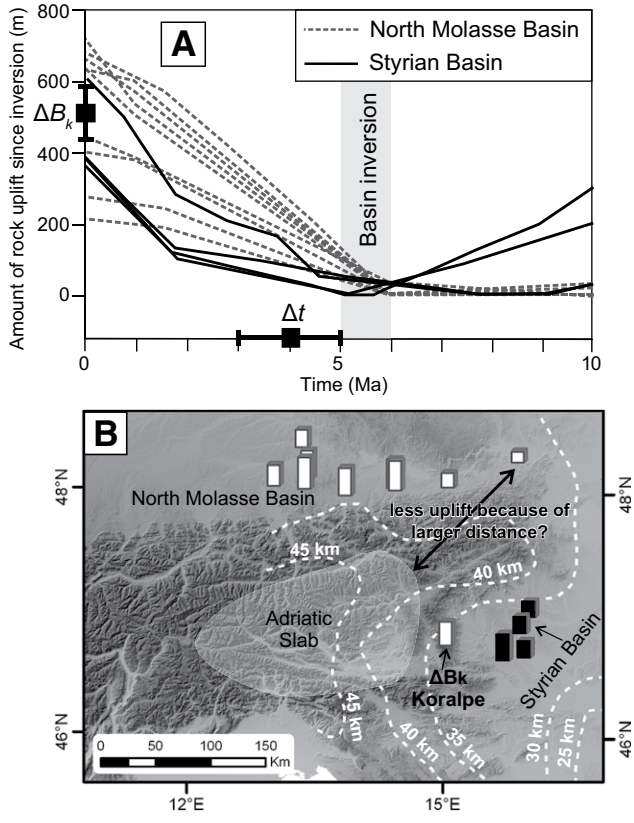

Figure 9. Vertical motions in the basins surrounding the eastern Alps and deep-seated structures underneath the eastern end of the Alps as potential candidates for the uplift event inferred herein. (A) Comparison between total amount of base-level fall calculated for Koralpe and amount of rock uplift since inversion of basin (Ebner and Sachsenhofer, 1995; Sachsenhofer et al., 1998; Genser et al., 2007); Δt refers to Δt_k. (B) Adriatic slab extent as inferred from high P-wave velocities in the depth slice of 135–165 km after Luth et al. (2013); dashed white lines are Moho depth contour lines after Brückl et al. (2010).

driver seems unlikely at the eastern end of the Alps. This region was well-removed from the main LGM ice body (Fig. 1), and post-LGM rebound due to ice unloading is limited to ~100 m (Sternai et al., 2012). Also, our calculated timing for the increase in rock uplift at 4 ± 1 Ma is significantly older than the onset of periodic glaciations (see also Cederbom et al., 2011). Thus, the recent increase in uplift of the Koralpe range documented here neither fits with the timing nor with the spatial occurrence of the last periodic glaciations in the Alps. However, the uplift and incision seem closely related to the inversion of the vertical motions of the Styrian and northern Molasse Basins from subsidence throughout the Miocene. We therefore suggest that the causes for the uplift event discussed here may be closely related to the causes for the inversion of the Pannonian Basin.

In this context, it is useful to use our calculation of Δt_k and the amount of incision Δz to provide a rough estimate of the topographic evolution of the Koralpe range since the late Miocene. The present-day relief of Koralpe (R_j), between the summit and the elevation of the Styrian Basin, is ~1800 m. By removing the amount of incision (Δz) from the present-day relief, we calculate an initial relief (R_i) of ~1450 m (Fig. 8). This simple calculation suggests that ~80% of Koralpe relief was present before the increase in rock uplift rate, and ~20% was created by incision after the rock uplift rate increased. If we assume a constant regional base level, the elevation of the Koralpe summit was around 1800 m elevation compared to its present-day elevation of 2140 m. Although this suggests that most of the topography of Koralpe was present before 4 Ma, the increase of relief of 20% since that time is significant.

A simple explanation for this postorogenic tectonic-related increase in rock uplift could be the ongoing slow crustal convergence between Adria and stable Europe measured from global positioning system measurements (Bus et al., 2009). However, in this context, foreland basins like the northern Molasse Basin should subside due to plate loading and not be uplifted, as pointed out by Genser et al. (2007). We can therefore exclude a direct link between the convergence between Adria and Europe and the post-Miocene uplift of the eastern end of the Alps and surrounding sedimentary basins. If uplift related to climate and to active convergence can both be excluded, a deep-seated process seems to be a likely possibility to explain the observed increase in rock uplift rate since the late Miocene. Such an explanation is supported by the large wavelength of the emerging uplift pattern of several hundreds of kilometers, as shown in Figure 9. The spatial correlation of the emerging uplift pattern correlates to some extent with the location of the Adriatic slab at depth (Luth et al., 2013) and suggests mantle-derived causes for the uplift. Lippitsch et al. (2003), Kissling et al. (2006), and Genser et al. (2007) provided various models on the topology of the mantle lithosphere beneath the eastern Alps, and we refrain from discussing mantle processes further in view of the geomorphic focus of this paper (Fig. 9B).

Comparison Between the Koralpe and the Formerly Glaciated Alps

The current erosion rates of the Koralpe are one order of magnitude lower than ^{10}Be-derived erosion rates from the western, central, and eastern Alps, where they are typically of the order of a few millimeters per thousand years (Delunel et al., 2010; Wittmann et al., 2007; Norton et al., 2010a, 2010b, 2011). Such difference could be explained by a greater extent of glacial erosion to the west, which may precondition topography (e.g., Norton et al., 2010a) and/or further drive uplift and postglacial erosion (e.g., Wittmann et al., 2007).

At the scale of the Alps, the amount of young surface uplift documented here (350 m) seems very modest compared to the present-day topography of the Alps, where many summits are well above 3500 m in elevation. Additional uplift of 350 m would only provide an increase of summit elevation of 10%. However, we speculate that it is possible that this 10% of tectonically driven additional uplift (as documented here) may have been critical to trigger the creation of the Alpine ice cap in the glacial periods by contributing to a positive feedback mechanism between the small-amplitude tectonic-related uplift documented here and the well-constrained climate-related uplift (Norton et al., 2010b; Sternai et al., 2012).

CONCLUSION

We summarize our results and interpretation as follows:

(1) The Koralpe and surrounding mountain ranges are the only peaks in the Alps that have summits above 2000 m surface elevation but were never pervasively ice covered during the glacial periods of the last 2 m.y. As such, they form one of the few locations within the range where glacial erosion was absent, and the geomorphology can be interpreted in terms of pre-Pleistocene processes.

(2) ^{10}Be-derived erosion rates from the Koralpe range are approximately one order of magnitude lower (36–149 m/m.y.) than erosion rates from previously glaciated regions of the Alps at similar elevation. However, there is a clear separation of relatively high erosion rates in what is interpreted as young, incised parts of the landscape (120–149 mm/k.y.) at low elevations and significantly lower erosion rates in the old relict landscape at high elevations (36–55 mm/k.y.). This confirms the interpretation that the Koralpe is a transient landscape that is currently responding to an increase in uplift rate that commenced only some few million years ago.

(3) The data allow us to calculate an onset of incision for the Koralpe range of 4 ± 1 Ma and amount of total relative base-level fall of 540 ± 140 m. These results fit with data sets from surrounding regions in the Styrian karst, the Styrian Basin, and the northern Molasse Basin and suggest a common rock uplift increase for the whole area at the end of the Miocene. Such a post-Miocene uplift event has been documented for the central Alps (e.g., Baran et al., 2014), but it is new for the eastern Alps.

(4) At the eastern end of the Alps, the post-Miocene uplift driver is unlikely to be directly due to active convergence between Adria and Europe or the result of a climatic change. We suggest that the increase in rock uplift rate may be due to a deep-seated process in the lithosphere, for example, thinning of the mantle part of the lithosphere by slab breakoff or delamination.

ACKNOWLEDGMENTS

This work was funded by the Topo-Alps project (Austrian Science Fund project I152-N19). We thank Hella Wittmann for laboratory support. Fritz Schlunegger, Paul Bierman, and three further anonymous reviewers are thanked for their thoughtful, positive, and constructive comments.

REFERENCES CITED

Abbühl, L.M., Norton, K.P., Jansen, J.D., Schlunegger, F., Aldahan, A., and Possnert, G., 2011, Erosion rates and mechanisms of knickzone retreat inferred from ^{10}Be measured across strong climate gradients on the northern and central Andes Western Escarpment: Earth Surface Processes and Landforms, v. 36, p. 1464–1473, doi:10.1002/esp.2164.

Auer, M., 2003, Regionalisierung von Schneeparametern—Eine Methode zur Darstellung von Schneeparametern im Relief: Bern, Switzerland, Universität Bern, 97 p.

Baran, R., Friedrich, A.M., and Schlunegger, F., 2014, The late Miocene to Holocene erosion pattern of the Alpine foreland basin reflects Eurasian slab unloading beneath the western Alps rather than global climate change: Lithosphere, v. 6, no. 2, p. 124–131, doi:10.1130/L307.1.

Brückl, E., Behm, M., Decker, K., Grad, M., Guterch, A., Keller, G.R., and Thybo, H., 2010, Crustal structure and active tectonics in the eastern Alps: Tectonics, v. 29, no. 2, TC2011, doi:10.1029/2009TC002491.

Bus, Z., Grenerczy, G., Tóth, L., and Mónus, P., 2009, Active crustal deformation in two seismogenic zones of the Pannonian region—GPS versus seismological observations: Tectonophysics, v. 474, p. 343–352, doi:10.1016/j.tecto.2009.02.045.

Carretier, S., Regard, V., Vassallo, R., Aguilar, G., Martinod, J., Riquelme, R., Pepin, E., Charrier, R., Herail, G., Farias, M., Guyot, J.-L., Vargas, G., and Lagane, C., 2013, Slope and climate variability control of erosion rates in the Andes of central Chile: Geology, v. 41, p. 195–198, doi:10.1130/G33735.1.

Cederbom, C.E., Sinclair, D.H., Schlunegger, F., and Meinert, K.R., 2004, Climate-induced rebound and exhumation of the European Alps: Geology, v. 32, p. 709–712, doi:10.1130/G20491.1.

Cederbom, C.E., van der Beek, P., Schlunegger, F., Sinclair, H.D., and Oncken, O., 2011, Rapid extensive erosion of the North Alpine foreland basin at 5–4 Ma: Basin Research, v. 23, p. 528–550, doi:10.1111/j.1365-2117.2011.00501.x.

Champagnac, J.D., Molnar, P., Anderson, R.S., Sue, C., and Delacou, B., 2007, Quaternary erosion-induced isostatic rebound and exhumation of the European Alps: Geology, v. 35, p. 195–198, doi:10.1130/G23053A.1.

Cloetingh, S., Bada, G., Maþenco, L., Lankreijer, A., Horváth, F., and Dinu, C., 2006, Neotectonics of the Pannonian-Carpathian system: Inferences from thermo-mechanical modelling, *in* Gee, D.G., and Stephenson, R.A., eds., European Lithosphere Dynamics: Geological Society of London Memoir 32, p. 207–221.

Delunel, R., van der Beek, P.A., Carcaillet, J., Bourles, D.L., and Valla, P.G., 2010, Frost-cracking control on catchment denudation rates: Insights from in situ produced ^{10}Be concentrations in stream sediments (Ecrins-Pelvoux massif, French western Alps): Earth and Planetary Science Letters, v. 293, p. 72–83, doi:10.1016/j.epsl.2010.02.020.

DiBiase, R.A., Whipple, K.X., Heimsath, A.M., and Ouimet, W.B., 2010, Landscape form and millennial erosion rates in the San Gabriel Mountains: Earth and Planetary Science Letters, v. 289, p. 134–144, doi:10.1016/j.epsl.2009.10.036.

Dunai, T.J., 2000, Scaling factors for production rates of in situ produced cosmogenic nuclides: A critical reevaluation: Earth and Planetary Science Letters, v. 176, p. 157–169, doi:10.1016/S0012-821X(99)00310-6.

Dunkl, I., Kuhlemann, J., Reinecker, J., and Frisch, W., 2005, Cenozoic relief evolution of the Eastern Alps—Constraints from apatite fission track age-provenance of Neogene intramontane sediments: Australian Journal of Earth Sciences, v. 98, p. 92–105.

Ebner, E., and Sachsenhofer, R.E., 1995, Paleogeography, subsidence and thermal history of the Neogene Styrian Basin (Pannonian Basin system, Austria), *in* Neubauer, E., Ebner, E., and Wallbrecher, E., eds., Tectonics of the Alpine-Carpathian-Pannonian Region: Tectonophysics, v. 242, p. 133–150.

Frisch, W., Kuhlemann, J., Dunkl, I., and Brügel, A., 1998, Palinspastic reconstruction and topographic evolution of the eastern Alps during the Late Tertiary extrusion: Tectonophysics, v. 297, p. 1–15, doi:10.1016/S0040-1951(98)00160-7.

Genser, J., Cloetingh, S., and Neubauer, F., 2007, Late orogenic rebound and oblique Alpine convergence: New constraints from subsidence analysis of the Austrian Molasse Basin: Global and Planetary Change, v. 58, p. 214–223, doi:10.1016/j.gloplacha.2007.03.010.

Granger, D.E., Kirchner, J.W., and Finkel, R., 1996, Spatially averaged long-term erosion rates measured from in situ–produced cosmogenic nuclides in alluvial sediment: The Journal of Geology, v. 104, p. 249–257, doi:10.1086/629823.

Hejl, E., 1997, "Cold spots" during the Cenozoic evolution of the eastern Alps: Thermochronological interpretation of apatite fission-track data: Tectonophysics, v. 272, p. 159–173, doi:10.1016/S0040-1951(96)00256-9.

Hergarten, S., Wagner, T., and Stüwe, K., 2010, Age and prematurity of the Alps derived from topography: Earth and Planetary Science Letters, v. 297, p. 453–460, doi:10.1016/j.epsl.2010.06.048.

Herman, F., Seward, D., Valla, P.G., Carter, A., Kohn, B., Willett, S.D., and Ehlers, T.A., 2013, Worldwide acceleration of mountain erosion under a cooling climate: Nature, v. 504, p. 423–426, doi:10.1038/nature12877.

Hurst, M.D., Mudd, S.M., Walcott, R., Attal, M., and Yoo, K., 2012, Using hilltop curvature to derive the spatial distribution of erosion rates: Journal of Geophysical Research, v. 117, p. F02017, doi:10.1029/2011JF002057.

Kirby, E., and Whipple, K.X., 2012, Expression of active tectonics in erosional landscapes: Journal of Structural Geology, v. 44, p. 54–75, doi:10.1016/j.jsg.2012.07.009.

Kissling, E., Schmid, S.M., Lippitsch, R., Ansorge, J., and Fügenschuh, B., 2006, Lithosphere structure and tectonic evolution of the Alpine arc: New evidence from high-resolution teleseismic tomography, *in* Gee, D.G., and Stephenson R.A., eds., European Lithosphere Dynamics: Geological Society of London Memoir 32, p. 129–145.

Kuhlemann, J., Frisch, W., Szekely, B., Dunkl, I., and Kazmer, M., 2002, Postcollisional sediment budget history of the Alps: Tectonic versus climatic control: International Journal of Earth Sciences, v. 91, p. 818–837, doi:10.1007/s00531-002-0266-y.

Kurz, W., Wölfler, A., Rabitsch, R., and Genser, J., 2011, Polyphase movement on the Lavanttal fault zone (eastern Alps): Reconciling the evidence from different geochronological indicators: Swiss Journal of Geosciences, v. 104, p. 323–343, doi:10.1007/s00015-011-0068-y.

Legrain, N., Stüwe, K., and Wölfler, A., 2014, Incised relict landscapes in the eastern Alps: Geomorphology, v. 221, p. 124–138, doi:10.1016/j.geomorph.2014.06.010.

Lippitsch, R., Kissling, E., and Ansorge, J., 2003, Upper mantle structure beneath the Alpine orogen from high-resolution teleseismic tomography: Journal of Geophysical Research, v. 108, no. B8, p. 2376, doi:10.1029/2002JB002016.

Luth, S., Willingshofer, E., Sokoutis, D., and Cloetingh, S., 2013, Does subduction polarity change below the Alps? Inferences from analogue modelling: Tectonophysics, v. 582, p. 140–161, doi:10.1016/j.tecto.2012.09.028.

Miller, S.R., Sakb, P.B., Kirby, E., and Bierman, P.R., 2013, Neogene rejuvenation of central Appalachian topography: Evidence for differential rock uplift from stream profiles and erosion rates: Earth and Planetary Science Letters, v. 369-370, p. 1–12, doi:10.1016/j.epsl.2013.04.007.

Montgomery, D., and Brandon, M., 2002, Topographic controls on erosion rates in tectonically active mountain ranges: Earth and Planetary Science Letters, v. 201, p. 481–489, doi:10.1016/S0012-821X(02)00725-2.

Neubauer, F., and Genser, J., 1990, Architektur und Kinematik der östlichen Zentralalpen—Eine Übersicht: Mitteilungen des Naturwissenschaftlichen Vereins für Steiermark, v. 120, p. 203–219.

Nishiizumi, K., Imamura, M., Caffee, M.W., Southon, J.R., Finkel, R.C., and McAninch, J., 2007, Absolute calibration of ^{10}Be AMS standards: Nuclear Instruments & Methods in Physics Research, Section B, Beam Interactions with Materials and Atoms, v. 258, p. 403–413, doi:10.1016/j.nimb.2007.01.297.

Norton, K.P., and Vanacker, V., 2009, Effects of terrain smoothing on topographic shielding correction factors for cosmogenic nuclide–derived estimates of basin-averaged denudation rates: Earth Surface Processes and Landforms, v. 34, p. 145–154, doi:10.1002/esp.1700.

Norton, K.P., Abbühl, L.M., and Schlunegger, F., 2010a, Glacial conditioning as an erosional driving force in the central Alps: Geology, v. 38, p. 655–658, doi:10.1130/G31102.1.

Norton, K.P., von Blanckenburg, F., and Kubik, P.W., 2010b, Cosmogenic nuclide–derived rates of diffusive and episodic erosion in the glacially sculpted upper Rhone Valley, Swiss Alps: Earth Surface Processes and Landforms, v. 35, p. 651–662.

Norton, K.P., von Blanckenburg, F., DiBiase, R., Schlunegger, F., and Kubik, P.W., 2011, Cosmogenic ^{10}Be-derived denudation rates of the eastern and southern European Alps: International Journal of Earth Sciences, v. 100, p. 1163–1179, doi:10.1007/s00531-010-0626-y.

Ratschbacher, L., Frisch, W., Linzer, H.G., and Merle, O., 1991, Lateral extrusion in the eastern Alps: Part 2. Structural analysis: Tectonics, v. 10, p. 257–271, doi:10.1029/90TC02623.

Reinhardt, L.J., Bishop, P., Hoey, T.B., Dempster, T.J., and Sanderson, D.C.W., 2007, Quantification of the transient response to base-level fall in a small mountain catchment: Sierra Nevada, southern Spain: Journal of Geophysical Research, v. 112, p. F03S05, doi:10.1029/2006JF000524.

Robl, J., Hergarten, S., and Stüwe, K., 2008, Morphological analysis of the drainage system in the eastern Alps: Tectonophysics, v. 460, p. 263–277, doi:10.1016/j.tecto.2008.08.024.

Sachsenhofer, R.F., Dunkl, I., Hasenhüttl, C., and Jelen, B., 1998, Miocene thermal history of the southwestern margin of the Styrian Basin: Vitrinite reflectance and fission-track data from the Pohorje/Kozjak area (Slovenia): Tectonophysics, v. 297, p. 17–29, doi:10.1016/S0040-1951(98)00161-9.

Schaller, M., von Blanckenburg, F., Veldkamp, A., Tebbens, L.A., Hovius, N., and Kubik, P.W., 2002, A 30,000 year record of erosion rates from cosmogenic ^{10}Be in middle European river terraces: Earth and Planetary Science Letters, v. 204, p. 307–320, doi:10.1016/S0012-821X(02)00951-2.

Scharf, A., Handy, M.R., Favaro, S., and Schmid, S., 2013, Modes of orogen-parallel stretching and extensional exhumation in response to microplate indentation and roll-back subduction (Tauern Window, eastern Alps): International Journal of Earth Sciences, v. 102, p. 1627–1654, doi:10.1007/s00531-013-0894-4.

Sternai, P., Herman, F., Champagnac, J.D., Fox, M.R., Salcher, B., and Willett, S.D., 2012, Pre-glacial topography of the European Alps: Geology, v. 40, p. 1067–1070, doi:10.1130/G33540.1.

Tenczer, V., and Stüwe, K., 2003, The metamorphic field gradient in the eclogite type locality: Journal of Metamorphic Geology, v. 21, p. 377–393, doi:10.1046/j.1525-1314.2003.00448.x.

Van den Berg, F., Schlunegger, F., Akçar, N., and Kubik, P., 2012, ^{10}Be-derived assessment of accelerated erosion in a glacially conditioned inner gorge, Entlebuch, central Alps of Switzerland: Earth Surface Processes and Landforms, v. 37, p. 1176–1188, doi:10.1002/esp.3237.

van Husen, D., 1997, LGM and late-glacial fluctuations in the eastern Alps: Quaternary Journal International, v. 38/39, p. 109–118, doi:10.1016/S1040-6182(96)00017-1.

von Blanckenburg, F., Hewawasam, T., and Kubik, P., 2004, Cosmogenic nuclide evidence for low weathering and denudation in the wet tropical highlands of Sri Lanka: Journal of Geophysical Research, v. 109, F03008, doi:10.1029/2003JF000049.

Wagner, T., Fabel, D., Fiebig, M., Häuselmann, P., Sahy, D., Xu, S., and Stüwe, K., 2010, Young uplift in the non-glaciated parts of the eastern Alps: Earth and Planetary Science Letters, v. 295, p. 159–169, doi:10.1016/j.epsl.2010.03.034.

Wagner, T., Fritz, H., Stüwe, K., Nestroy, O., Rodnight, H., Hellstrom, J., and Benischke, R., 2011, Correlations of cave levels, stream terraces and planation surfaces along the River Mur. Timing of landscape evolution along the eastern margin of the Alps: Geomorphology, v. 295, p. 159–169.

Whipple, K.X., and Tucker, G.E., 1999, Dynamics of the stream-power river incision model: Implications for height limits of mountain ranges, landscape response timescales and research needs: Journal of Geophysical Research, v. 104, p. 17,661–17,674, doi:10.1029/1999JB900120.

Willett, S.D., 2010, Late Neogene erosion of the Alps: A climate driver?: Annual Review of Earth and Planetary Sciences, v. 38, p. 411–437, doi:10.1146/annurev-earth-040809-152543.

Winkler-Hermaden, A., 1957, Geologisches Kräftespiel und Landformung: Vienna, Austria, Springer Verlag, 822 p.

Wittmann, H., von Blanckenburg, F., Kruesmann, T., Norton, K.P., and Kubik, P.W., 2007, Relation between rock uplift and denudation from cosmogenic nuclides in river sediment in the central Alps of Switzerland: Journal of Geophysical Research, v. 112, p. F04010, doi:10.1029/2006JF000729.

Wobus, C., Whipple, K.X., Kirby, E., Snyder, N., Johnson, J., Spyropolo, K., Crosby, B., and Sheehan, D., 2006, Tectonics from topography: Procedures, promise and pitfalls, *in* Willett, S.D., Hovius, N., Brandon, M.T., and Fisher, D.M., eds., Tectonics, Climate, and Landscape Evolution: Geological Society of America Special Paper 398, p. 55–74.

MANUSCRIPT RECEIVED 12 MAY 2014
REVISED MANUSCRIPT RECEIVED 22 SEPTEMBER 2014
MANUSCRIPT ACCEPTED 1 OCTOBER 2014

Printed in the USA

Lithosphere

Post-Miocene landscape rejuvenation at the eastern end of the Alps

Nicolas Legrain, Jean Dixon, Kurt Stüwe, Friedhelm von Blanckenburg and Peter Kubik

Lithosphere 2015;7;3-13
doi: 10.1130/L391.1

Notes